Exclusive-final-state hadron observables from neutrino-nucleus multinucleon knockout

J. E. Sobczyk,[1,2] J. Nieves,[1] and F. Sánchez[3]

[1]*Instituto de Física Corpuscular (IFIC), Centro Mixto CSIC-Universidad de Valencia, Institutos de Investigación de Paterna, Apartado 22085, E-46071 Valencia, Spain*

[2]*Institut für Kernphysik and PRISMA⁺ Cluster of Excellence, Johannes Gutenberg-Universität Mainz, 55128 Mainz, Germany*

[3]*Université de Genève, Faculté des Sciences, Département de Physique Nucléaire et Corpusculaire (DPNC) 24, Quai Ernest-Ansermet, CH-1211 Genève 4, Switzerland*

(Received 24 February 2020; revised 29 May 2020; accepted 10 July 2020; published 3 August 2020)

We present results of an updated calculation of the two particle two hole (2p2h) contribution to the neutrino-induced charge-current cross section. We provide also some exclusive observables, interesting from the point of view of experimental studies, e.g., distributions of momenta of the outgoing nucleons and of available energy, which we compare with the results obtained within the NEUT generator. We also compute, and separate from the total, the contributions of 3p3h mechanisms. Finally, we discuss the differences between the present results and previous implementations of the model in MC event generators, done at the level of inclusive cross sections, which might significantly influence the experimental analyses, particularly in the cases where the hadronic observables are considered.

DOI: 10.1103/PhysRevC.102.024601

I. INTRODUCTION

The studies of neutrino-nucleus interactions are entering a new stage, motivated by long-baseline experimental programs, in which the statistical uncertainties will diminish and thus the nuclear effects—contributing to the systematical error—have to be kept well under control [1]. The incomplete theoretical knowledge of the neutrino-nucleus interactions influences various stages of experimental analysis. For instance, for the future Hyper-Kamiokande water Cherenkov detector, the reconstruction of neutrino energy will be mainly based on the kinematical method, in which only the outgoing muon is observed and the reaction kinematics is assumed to be quasielastic (QE). However, the energy range of the neutrino flux produced in the Japan Proton Accelerator Research Complex facility is such that other physical mechanisms give a nonnegligible contribution to the cross section. In particular, multinucleon knockout processes [mainly driven by the excitation of two particle-two hole (2p2h) components in nuclei] should be taken into account. Since in the latter processes the interaction takes place on a pair of nucleons, the energy balance is different than in the QE case. Mismatching the signal coming from these two reaction mechanisms would lead to a bias in the energy reconstruction [2,3]. It is therefore crucial to properly include the 2p2h channel into the Monte Carlo event generators.

Various theoretical groups have presented calculations for 2p2h contributions, providing mainly the results for inclusive cross sections. There is an ongoing discussion on the treatment of this physical reaction. The topic, primarily explored theoretically few decades ago in the case of electron scattering, has found recently a new application for neutrino-nucleus interactions. The computation requires multidimensional phase-space integration and the inclusion of $\Delta(1232)$ degrees of freedom. Most of the 2p2h approaches start from the in-medium calculation of the meson exchange currents (MEC) between two nucleons, mediated via one pion. However, this treatment, in which a pion is the principal carrier of interaction, though adequate in the free space for moderate energies, requires substantial modifications inside of the nuclear medium, where the situation becomes more complicated. The nuclear effects are modelled differently in various approaches.

The response functions for one- and two-body currents obtained from *ab initio* calculations using the Green-function Monte Carlo (GFMC) approach were presented in Ref. [4]. They may be treated as a benchmark for more approximated and phenomenological models, although there are two serious drawbacks from the point of view of experimental needs. First, the calculations are constrained to a limited phase space where the nonrelativistic kinematics can be employed (nuclear correlations and electroweak currents are nonrelativistic). Second, such approach provides only inclusive cross sections, without predicting the spectrum of outgoing nucleons. Very recently, an *ab initio* calculation of the neutrino flux-folded inclusive cross sections, measured on ^{12}C by the MiniBooNE [5,6] and T2K [7] collaborations in the charged-current quasielastic QE regime has appeared [8]. The calculation is based on realistic two- and three-nucleon interactions and on a realistic nuclear electroweak current with one- and two-nucleon terms that are constructed consistently with these interactions and reproduce low-energy electroweak transitions. Numerically exact quantum Monte Carlo methods are utilized to compute the nuclear weak response functions by fully retaining many-body correlations in the initial and final states and interference effects between one- and two-body current contributions. This sophisticated theoretical framework is an important step

forward, but it also suffers from the limitations mentioned above. Furthermore, it does not account for explicit pion production mechanisms and therefore cannot describe the nuclear electroweak response in the Δ resonance region and beyond. In addition, the quantum Monte Carlo can be only applied to light nuclei ($A \leqslant 12$).

Among other more phenomenological schemes, the model of Refs. [9,10] was the first one to be proposed for neutrino-nucleus 2p2h contributions. Conceptually it is closely related to the approach followed in the present work, with the computation of some many-body diagrams, including some Δh effects with the Δ self-energy in the nuclear medium obtained within the same formalism of Ref. [11]. The difference lies in the treatment of the nonresonant background contributions, which in these works were extrapolated from previous 2p2h calculations, either for pion absorption at threshold [12] or for the (e, e') inclusive reaction [13].

Recently, an extension of electron-nucleus 2p2h calculation of Ref. [14] has been presented for the charge current (CC) and the neutral current (NC) cases [15]. In this approach, the correlations of the ground state are accounted for by means of hole spectral functions of both nucleons (the difference from the two-nucleon spectral function has been advocated to be small). The Δ exchange is parametrized as in Ref. [16], but only one-pion exchange between the nucleons is considered. The approach of Ref. [17] is based on the same set of exchange currents as in Ref. [15], though no correlations between initial nucleons are included (i.e., they are distributed according to the Fermi gas model).

Here we follow the formalism derived in Ref. [18], which, together with Refs. [9,10], provided the first sensible theoretical explanation [19,20] for the so-called MiniBooNE axial mass puzzle [5]. This theoretical calculation is widely used by the experimental community and it has been included into several MC event generators; still only at the level of inclusive cross sections, with the outgoing nucleons (produced at the primary vertex of interaction) being distributed isotropically according to the available phase space and cascaded through the nucleus by means of a Monte Carlo algorithm. The final distributions, however, are only an approximation which does not fully take into account the internal dynamics of the process.

We perform here a comparison between the results of exclusive final-state hadron distributions, as they are obtained within the full model after undoing the outgoing nucleon phase-space integration and as they are implemented in the NEUT generator [21]. For the first time we also show the results of the model separately for the 2p2h and 3p3h contributions, which until now were treated together. This way we are able to make predictions of exclusive two-nucleon final states. We also improve on the previous treatment of the in-medium interactions between nucleons and Δ's, maintaining the energy-transfer dependence of g'_l and g'_t, the longitudinal and transverse Landau-Migdal parameters of the effective nucleon-nucleon spin-isospin interaction [11]. The treatment of the Δ resonance is also refined according to recent work (including changes in the Δ propagator and in the dominant $C_5^A(q^2)$ electroweak form factor [22]). In addition, the whole calculation is performed without the numerical approximations used in the previous work of Ref. [18]. Indeed, this work serves as a further validation of the previous calculation. Since there have been tensions observed between various theoretical approaches [23], we find both this confirmation and some further improvements of the model an important step forward.

As noted in Ref. [14], the interference between amplitudes involving one- and two-nucleon currents might play an important role. The results of a calculation [24] of the transverse electromagnetic response of ^{4}He and of the corresponding sum rule of ^{12}C, evaluated using state-of-the-art models of the nuclear Hamiltonian and currents, within the GFMC computational scheme are used in Ref. [14] to support such conclusion. The recent work of Ref. [8] reinforces this scenarios, with this interference leading to a significant increase in the cross-section results obtained in impulse approximation and becoming important for bringing theory into much better agreement with MiniBooNE and T2K experiments.

The theoretical framework used in this work for the initial weak step does not include all the interference terms analyzed in Refs. [8,14]. Roughly, the scheme takes into account processes which are triggered by MEC, leaving out others, e.g., interference contributions between initial ground-state correlations (ISC) and MEC terms, which also lead to QE-like (pionless) events. As we will discuss in some detail below, in a first step, the model assumes a counting scheme based on the number of hole lines, related to an expansion in density. Later, some resummations, in the random phase approximation (RPA) sense and driven by the in-medium NN, $N\Delta(1232)$, and $\Delta\Delta$ effective interactions, are performed. Within this scheme, the ISC-related contributions appear at higher orders than those from final-state correlations (FSC) and MEC many-body diagrams. Effects due to ISC could be in principle implemented going to higher orders in the density expansion. Besides technical issues, one would face an additional problem. The nuclear model for excitation of 2p2h components has some effective parameters [e.g., short-distance Landau-Migdal parameters in the NN, $N\Delta(1232)$ and $\Delta\Delta$ interactions, mentioned above], which were adjusted in the late 1980s to some data [25–27], and their phenomenological values could effectively account for neglected higher-order corrections to some extent, as it occurs in any counting scheme when it is truncated. Indeed, this seems very possible, given the phenomenological success of the scheme, not only for pion-nuclear reactions but also for inclusive photon-, electron-, and (anti-)neutrino processes, including the reproduction of the MiniBooNE CCQE-like double-differential cross sections [18–20,28–30]. Therefore, including higher-order many-body contributions to the original model would necessarily require a new fit of the effective parameters to a large sample of pion-, photon-, and electron-nuclear cross-section data. This is beyond the scope of the present work, where we have focused on evaluating how various two-nucleon knockout distributions are affected by the Monte Carlo cascade used to account for the interactions of the outgoing nucleons, through their path leaving out the nucleus. We provide different spectra that can be directly confronted with experiment and that further test different aspects of the approach (e.g., isospin dependence, excitation of $\Delta(1232)$ components, 3p3h contributions, etc.).

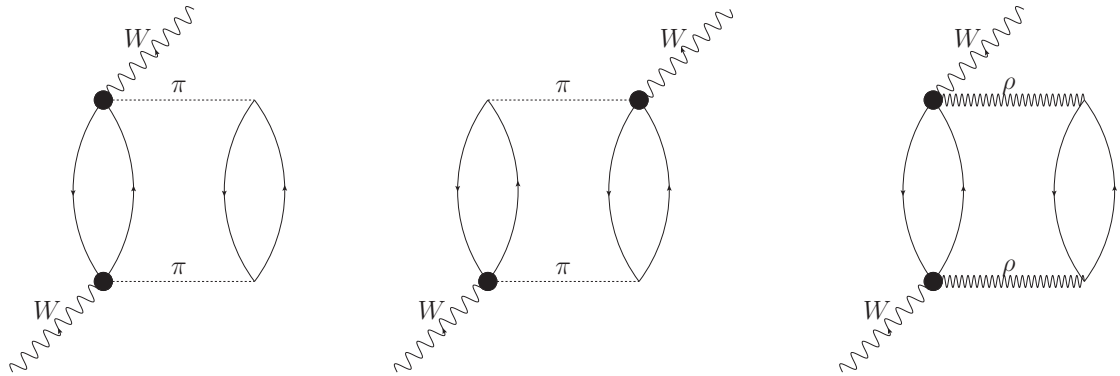

FIG. 1. Different 2p2h contributions to the W^+ self-energy in the nuclear matter driven by pion and ρ exchanges and which are taken into account in our work in a first step. The full circles account for the $WN \to \pi N$ and $WN \to \rho N$ amplitudes [18]. In some terms the π and ρ exchanges are supplemented by short-range correlations, and, finally, the in-medium interactions are obtained after performing some resummations, in the RPA sense and driven by effective NN, $N\Delta(1232)$, and $\Delta\Delta$ potentials (see Refs. [18,25,38] for details). The hole (particle) states are denoted with downward (upward) arrows.

This work is organized in the following way. In Sec. II we sketch the formalism. First, in Sec. II A, we present how the nuclear correlation effects, and their interplay with MEC, are included in our framework. Then we concentrate on the description of the in-medium baryon-baryon effective interaction in Sec. II B and the treatment of Δ self-energy and propagator in Secs. II C and II D. We also pay attention to the 3p3h mechanism in Sec. II E. Next, in Sec. III we shortly describe how the model and final-state interactions are implemented in NEUT event generator. The results are presented in Sec. IV. First, we focus on the inclusive cross sections to understand the effect of the various refinements introduced in the model. Afterward we present the distributions of outgoing nucleons and an analysis of the available energy. The conclusions and outlook are presented in Sec. V.

II. FORMALISM

The multinucleon knockout formalism we employ is based on the approach introduced for neutrino-nucleus interaction for the first time in Ref. [18]. In the past, the model has been extensively used for electron-, photon-, and pion-nucleus scattering and proved to describe the available data with a good accuracy [28–30].

The approach makes use of the local density approximation, in which the nucleus is locally treated as the nuclear medium of constant density, to obtain results for finite nuclei from nuclear matter calculations. In one of the most important reaction mechanisms at intermediate energy transfers, the mediator of electroweak interactions, the $W^\pm$ boson for CC interactions, traveling through the nuclear environment is absorbed by a pair of nucleons, producing another two. We will call this mechanism 2p2h.[1] The interaction between two particle-hole excitations (ph-ph), in the spin-isospin channel, can be separated into the longitudinal and the transverse channels. These are triggered by one-pion and ρ exchanges, respectively; with in-medium corrections which strongly influence both channels. To be precise, in a first step the many-body diagrams calculated are shown in Fig. 1. The structure of the $W^\pm N \to \pi N$ and $W^\pm N \to \rho N$ amplitudes can be found in Refs. [18,22]. It is worth mentioning that recently an extensive comparison of the electroweak pion production in the dynamical coupled-channels (DCC) model [31,32], Sato-Lee model [33–36], and the model of Refs. [18,22] has been performed [37]. It has been shown that the latter approach—in spite of its simplicity—recovers the bulk of physical properties in the kinematical region of $\Delta(1232)$ excitation. This fact may serve as a confirmation that the model for the $W^\pm N \to \pi N$ reaction used in the present work for the 2p2h calculation is trustworthy.

We will focus on the inclusive nuclear reaction

$$\nu_l(k) + A_Z \to l^-(k') + X \tag{1}$$

driven by the electroweak CC. The double differential cross section, with respect to the outgoing lepton kinematical variables, for the process of Eq. (1) is given in the laboratory (LAB) frame by

$$\frac{d^2\sigma_{\nu l}}{d\Omega(\hat{k}')dE'_l} = \frac{|\vec{k}'|}{|\vec{k}|}\frac{G^2}{4\pi^2}L_{\mu\sigma}W^{\mu\sigma} \tag{2}$$

with $\vec{k}$ and $\vec{k}'$ the LAB lepton momenta, $E'_l = (\vec{k}'^2 + m_l^2)^{1/2}$ and m_l the energy and the mass of the outgoing lepton, $G = 1.1664 \times 10^{-11}$ MeV^{-2}, the Fermi constant, and L and W the leptonic and hadronic tensors, respectively. The leptonic tensor is given by:[2]

$$\begin{aligned} L_{\mu\sigma} &= L^s_{\mu\sigma} + \mathrm{i}L^a_{\mu\sigma} \\ &= k'_\mu k_\sigma + k'_\sigma k_\mu - g_{\mu\sigma}k\cdot k' + \mathrm{i}\epsilon_{\mu\sigma\alpha\beta}k'^\alpha k^\beta. \end{aligned} \tag{3}$$

The hadronic tensor corresponds to the charged electroweak transitions of the target nucleus, i, to all possible final states.

[1] In the past, under this label we also referred to the absorption by three nucleons since it is included in the Δ self-energy. Here we will treat this mechanism separately and denote it as 3p3h.

[2] We take $\epsilon_{0123} = +1$ and the metric $g^{\mu\nu} = (+,-,-,-)$.

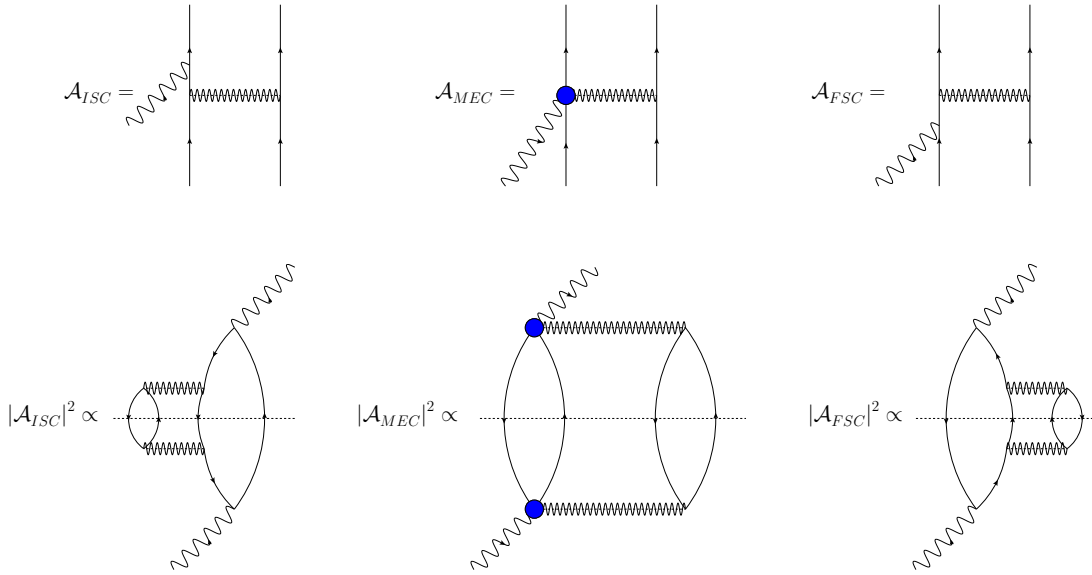

FIG. 2. Feynman open (first row) and many-body (second row) diagrams for three possible 2p2h mechanisms: diagonal ISC, MEC, and FSC terms. In the second row, horizontal dotted lines stand for the Cutkosky cuts which put on the mass shell the 2p2h excitation. The blue dots in the MEC diagrams stand for a general interaction vertex, which in our model consists of five contributions: Δ and crossed-Δ exchange, pion in flight, pion pole, and contact term (see Fig. 2 in Ref. [18]). The baryon-baryon interactions are described in Sec. II B and include both short- and long- (RPA) range correlations.

Expressions for the hadron tensor corresponding to the 2p2h diagrams in Fig. 1 can be found in Eqs. (27), (35), (36), and (40) of Ref. [18]. However, in the calculations presented in this work we will not perform an average over the initial nucleons momenta that appear in the electroweak amplitudes, as done in Ref. [18] [see the discussion around Eqs. (18) and (19) in the latter reference]. As was explained there, the difference between this approximated calculation and the full one is not large for inclusive cross sections. Here, however, we want to analyze exclusive hadronic final states which might be more sensitive to the averages done in the integrations. Let us also notice that in this way we automatically include the integration of Eq. (31) of Ref. [18] which was introduced to deal with the pole of nucleon propagator (see the discussion above Eq. (31) of Ref. [18]).

A. Initial- and final-state correlations

Having said what the classes of diagrams included in the formalism adopted here are, depicted in Fig. 1 and described in more detail in Ref. [18], we discuss the framework in a more general context of nuclear reactions, for which both the initial and final many-body states are composed of correlated nucleons. The effects of these correlations can be rigorously taken into account in a variety of *ab initio* approaches which recently have reached maturity to be able to calculate many-body nuclear transitions triggered by external electroweak probes [8]. Nevertheless, as already mentioned, these calculations are still limited by the size of nuclear system and transferred energies by the problems to properly account for pion production and the excitation of Δ degrees of freedom. In addition, they can be applied only to predict inclusive cross sections, while we aim here at obtaining outgoing nucleon distributions, which can be also confronted with data.

Some more phenomenological treatments might work better in regards to these limitations, at the price of only partially or effectively taking into account some of the correlation effects. In the approach used in this work [18,25], correlations beyond the statistical ones are neglected in the distribution of initial nucleons. Within the local density approximation, the nuclear density is treated as a small expansion parameter, which can be translated into the number of hole state propagators involved in each diagram. This guides us to sum classes of diagrams which give important contributions to the cross section, while neglecting others, with larger number of hole state propagators [25,39] (see also Ref. [40]).

With this in mind, let us consider in Fig. 2 three contributions to the inclusive nuclear cross section, for which the W gauge boson gets absorbed by two nucleons in the primary (weak) reaction. Looking at the open diagrams shown in the first row of the figure, we see that the first and third ones account for nuclear effects due to ISC and FSC, respectively, of the involved nucleons, this is, absorption by a pair of correlated nucleons. The second diagram stands for a MEC mechanism, where the W emits a virtual pion (pion pole) or is absorbed by an exchanged pion (pion in flight) or its absorption involves an N-to-Δ transition. There is also a contact term, required by chiral symmetry, in the model for MEC [16]. In the second row of Fig. 2, we show the corresponding many-body diagrams associated to the squared amplitudes of those depicted in the first row, when they are cut by the horizontal dotted line and the 2p2h are placed on shell (Cutkosky's rule). In addition, one has to take into account all possible interference terms, for instance, the two diagrams

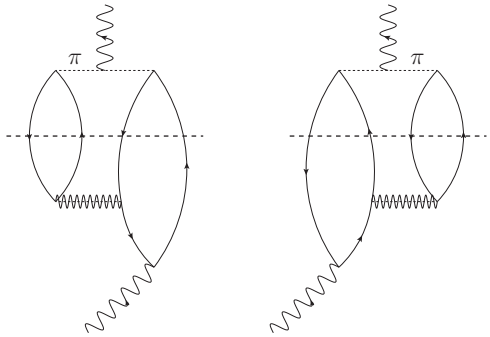

FIG. 3. Many-body diagrams accounting for the interference between the open ISC (left) and FSC (right) terms and the pion in flight MEC mechanism.

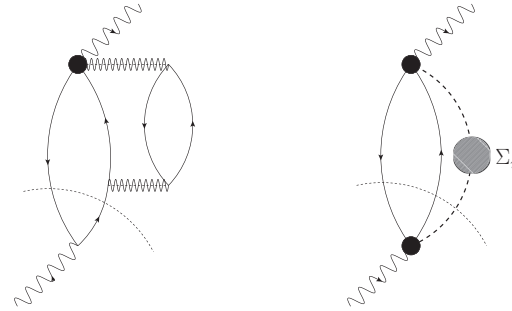

FIG. 4. Some diagram cuts providing further contributions to the inclusive lepton cross section. They may also lead to two nucleons in the final state, after considering secondary collisions. The Cutkosky cut (dotted line) puts on shell 1p1h state (left diagram) or 1p1h1π (right diagram). The full circles account for the $WN \to \pi N$ and $WN \to \rho N$ amplitudes [18].

depicted in Fig. 3, which denote, in the many-body language, the interference between the open ISC (left panel) and FSC (right panel) terms and the pion in flight MEC mechanism.

We emphasize at this point that the theoretical nucleon distributions obtained from this first step, where the W is absorbed, should not be directly compared with experiment. This is because the primary outgoing nucleons experience collisions, which produce changes of their energy, direction, and charge during their way out of the nucleus. These secondary nuclear collisions (SNC), which do not change the inclusive lepton cross sections, can appreciably distort the measurable nucleon spectra and are taken into account in this work by means of an intranuclear Monte Carlo cascade (alternatively, they can by described using quantum transport [41]).

Following the power-counting scheme established in Refs. [25,39], the lowest-order contributions come from the many-body diagrams containing only two hole propagators, as the middle and right ones of Fig. 2, and are originated from MEC and FSC terms and the interference between them. We consider these in our theoretical framework.[3] On the other hand, the ISC term (left diagram in the second row of Fig. 2) is driven by the ph contribution to the self-energy of the hole state. We note that it is of higher order in the density expansion since it contains four hole lines, and it has been neglected in the present calculation. The ISC and FSC diagrams in Fig. 2 provide imaginary contributions to nucleon's self-energy and hence to the hole and particle spectral functions, respectively [45,46]. We need only the imaginary parts of the many-body diagrams to account for the W absorption by two nucleons.

[3]Note that the diagonal FSC diagram (right one in Fig. 2) can be cast as 1p1h term, where the particle nucleon is dressed with a complex self-energy, Σ, and it is accounted for in QE calculations using spectral functions [42–45]. As discussed in Ref. [45], ReΣ acts as an energy-dependent effective potential which changes the in-medium dispersion relation of the nucleons in the weak WNN vertex. In turn, the imaginary part (ImΣ) accounts for NN collisions, being much larger for particle than for hole states [46], as expected from the counting in the number of hole-lines. Thus, the events induced by the imaginary part of the self-energy (driven by collisional broadening) should be treated separately, in the intranuclear cascade, from one-body events in the primary reaction.

These diagrams provide also real parts which together with the one-body contributions (e.g., Hartree-type terms) change the dispersion relation of the particle and hole inside of the nuclear medium. The use of a precise dispersion relation has been shown to be quite important to describe nuclear electroweak reactions, and it is commonly implemented by using realistic particle and hole spectral functions [42–45]. By neglecting the ISC diagram in Fig. 2, we are only neglecting the two-nucleon tail of the hole spectral function. For the sake of clarity, we mention that it is also common to refer as final-state interaction to the inclusion of nuclear corrections derived from the use of a realistic particle spectral function, which would contain both real and imaginary parts of the FSC diagram in Fig. 2.

Let us pay now attention to interference terms, for instance, to the two diagrams depicted in Fig. 3. We see that the ISC-MEC (left) and FSC-MEC (right) diagrams contain three and two hole propagators, respectively. Hence, within the counting scheme, the ISC-MEC interference diagram is of higher order than the latter one, and it was also neglected in Ref. [19] and in this work. The left diagram in Fig. 4 represents an FSC-MEC interference term and by means of the general vertex contains also the contribution depicted on the right panel of Fig. 3. It provides two different inclusions to the cross section. The first one is obtained when the 2p2h excitation is put on the mass shell, with the same cut as in the right panel of Fig. 3. This is included in the analysis carried out in this work. The second one is marked by the circular Cutkosky cut, and it amounts to placing the lower ph excitation on shell. This new source of imaginary part produces strength in the quasielastic peak [28]. The diagram with the circular cut could be then considered an ordinary ph excitation with a renormalized vertex. It can be also seen as the interference between amplitudes involving one- and two-nucleon currents, which following Refs. [4,8,14] lead to a significant increase in the inclusive cross-section results obtained in impulse approximation. Such mechanisms can also give rise to visible signatures of two nucleons due to the SNC of the primary nucleon, while it travels out of the nucleus. They will provide nucleon energy distributions that can be understood in terms of their QE origin and well

separated from those where the Δ resonance is excited or 3p3h components are sizable. Being interested in this work in the latter features, we have not considered such contributions, and we have always required an on-shell 2p2h excitation in the first step.

SNC also give rise to two-nucleon final state for other dynamical mechanisms. As an example, in the right panel of Fig. 4 we show a diagram-cut standing for a 1p1h1π mechanism, with the produced pion dressed (Σ_π) in the nuclear medium, which is not taken into account in the present calculation of two-nucleon distributions. Such contribution to the CC (anti-)neutrino inclusive cross sections was computed in Ref. [18]. However, the outgoing (real) pion after the first step, $WN \to N\pi$, might be absorbed before leaving out the nucleus, leading to a QE-like event, and without changing the inclusive cross section. These mechanisms, with a two-nucleon final state, are not considered in the present calculation of the outgoing nucleon spectra. This is also the case in the original works of Refs. [19,20], and is justified because the MiniBooNE Collaboration subtracted (using MC) these events in the published QE-like double-differential data samples.

In summary, we should acknowledge that the mechanisms considered in this work are not the only ones which might result in the two-nucleon final state. There are some 2p2h many body diagrams, mainly involving ISC, which are of higher order in the adopted expansion and have been neglected [40]. As mentioned in the Introduction, the systematic inclusion of such contributions is not trivial because of the presence of effective parameters in the theoretical framework used in this work. In addition, one should also consider 1p1h or 1p1h1π W-absorption modes in the primary vertex and follow secondary interactions in the nucleus, which may also lead to two visible nucleons in the detector.

B. In-medium baryon-baryon effective interaction in the spin-isospin channel

The key point of the approach is the assumption that the interaction between ph(Δh)-ph(Δh) nuclear excitations in the spin-isospin channel is originated from the π and the ρ exchanges and modified in the nuclear medium [11]. The one-pion exchange potential between two nucleons has a longitudinal character and is given in momentum space by

$$V_\pi(p) = \frac{f^2_{\pi NN}}{m^2_\pi} F^2_\pi(p^2)\, \vec{p}^{\,2} D_\pi(p^2)\, (\vec{\sigma}_1 \cdot \hat{p})\, (\vec{\sigma}_2 \cdot \hat{p})\, \vec{\tau}_1 \cdot \vec{\tau}_2 \quad (4)$$

with $\hat{p} = \vec{p}/|\vec{p}\,|$ the unitary three-momentum transfer and σ_i and τ_i ($i = 1, 2$) Pauli matrices acting on the spin and isospin nucleon degrees of freedom, respectively. In addition,

$$D_\pi(p^2) = \frac{1}{p^2 - m^2_\pi + i\epsilon}\,, \quad F_\pi(p^2) = \frac{\Lambda^2_\pi - m^2_\pi}{\Lambda^2_\pi - p^2}\,,$$
$$\Lambda_\pi = 1200\ \text{MeV}\,, \quad m_\pi = 139\ \text{MeV}. \quad (5)$$

We introduced the $F_\pi(p^2)$ form factor to account for off-shell effects on the πNN vertex and $f^2_{\pi NN}/4\pi = 0.08$. The potential $V_\pi(p)$ can be split into scalar and tensor parts:

$$(\vec{\sigma}_1 \cdot \hat{p})\, (\vec{\sigma}_2 \cdot \hat{p}) = \tfrac{1}{3}\vec{\sigma}_1 \cdot \vec{\sigma}_2 + \tfrac{1}{3} S_{12}(\hat{p}), \quad (6)$$

with the tensor operator $S_{12}(\hat{p}) = 3(\vec{\sigma}_1 \cdot \hat{p})\, (\vec{\sigma}_2 \cdot \hat{p}) - \vec{\sigma}_1 \cdot \vec{\sigma}_2$. The Fourier transform to the coordinate space, in the static limit ($p^0 = 0$) and neglecting the $F_\pi(p^2)$ form factor, of the scalar potential gives rise to

$$V_\pi(\vec{r}\,) = \frac{1}{3}\frac{f^2_{\pi NN}}{m^2_\pi}\left[\delta^3(\vec{r}\,) - \frac{m^2_\pi}{4\pi}\frac{e^{-m_\pi|\vec{r}|}}{|\vec{r}|}\right]\vec{\sigma}_1 \cdot \vec{\sigma}_2\ \vec{\tau}_1 \cdot \vec{\tau}_2, \quad (7)$$

with $|\vec{r}|$ the NN relative distance. The term proportional to $\delta^3(\vec{r}\,)$ comes from the construction of the potential when nucleons are treated as pointlike particles. This is not a correct physical behavior and it is first corrected by the form factor $F_\pi(p^2)$. Nevertheless, it is well known that the strong short-range correlations prevent nucleons from getting close to each other, and thus at shorter distances, a two-pion exchange mechanism gains in importance. One-pion exchange describes the long-range part of interaction, corresponding to distances $|\vec{r}\,| \geqslant \lambda_\pi = \frac{1}{m_\pi} \approx 1.4$ fm. Moreover, short-range correlations are modified inside of the nuclear medium.

In addition, the vector-isovector channel of the NN interaction is also strongly influenced by the ρ meson (transverse) exchange:

$$V_\rho(p) = C_\rho \frac{f^2_{\pi NN}}{m^2_\pi} F^2_\rho(p^2)\, \vec{p}^{\,2} D_\rho(p^2)\, (\vec{\sigma}_1 \times \hat{p})\, (\vec{\sigma}_2 \times \hat{p})\, \vec{\tau}_1 \cdot \vec{\tau}_2 \quad (8)$$

with

$$D_\rho(p^2) = \frac{1}{p^2 - m^2_\rho + i\epsilon}\,, \quad F_\rho(p^2) = \frac{\Lambda^2_\rho - m^2_\rho}{\Lambda^2_\rho - p^2}\,,$$
$$\Lambda_\rho = 2500\ \text{MeV}\,, \quad m_\rho = 770\ \text{MeV}\,, \quad C_\rho = 2. \quad (9)$$

Again, it can be separated into the scalar and tensor parts,

$$(\vec{\sigma}_1 \times \hat{p})\, (\vec{\sigma}_2 \times \hat{p}) = \tfrac{2}{3}\vec{\sigma}_1 \cdot \vec{\sigma}_2 - \tfrac{1}{3} S_{12}(\hat{p}), \quad (10)$$

with the former one also giving rise to a nonregularized $\delta^3(\vec{r}\,)$ term. On the other hand, the tensor components have an opposite sign for longitudinal and transverse parts and thus partially cancel [compare Eqs. (6) and (10)]. The approach of describing the nucleon-nucleon interaction in terms of meson exchanges breaks down at short distances where the potential is known to be strongly repulsive.[4] At this stage we follow Ref. [11] and introduce the effective terms g'_l and g'_t to account for short-range effects of the NN $\sigma\sigma\tau\tau$ interaction, such as multipole pion exchange, inside of the nuclear medium,

$$V(p) = V_\pi(p) + V_\rho(p) + \frac{f^2_{\pi NN}}{m^2_\pi} g'_l(p)\, (\vec{\sigma}_1 \cdot \hat{p})\, (\vec{\sigma}_2 \cdot \hat{p})\, \vec{\tau}_1 \cdot \vec{\tau}_2$$
$$+ C_\rho \frac{f^2_{\pi NN}}{m^2_\pi} g'_t(p)\, (\vec{\sigma}_1 \times \hat{p})\, (\vec{\sigma}_2 \times \hat{p})\, \vec{\tau}_1 \cdot \vec{\tau}_2. \quad (11)$$

To obtain g'_l and g'_t, we follow the discussion of Ref. [47], where a phenomenological correlation function $\Omega(\vec{r}\,)$ was

[4] In the calculations presented in this work the main strength will come from low and medium values of transferred momenta $\vec{p}$ between nucleons (for neutrinos $E_\nu \leqslant 2$ GeV, $|\vec{p}\,|$ peaks below 0.5 GeV, see the right panel in Fig. 5). These values of momenta probe mainly the region described by one- and two-pion exchange potential.

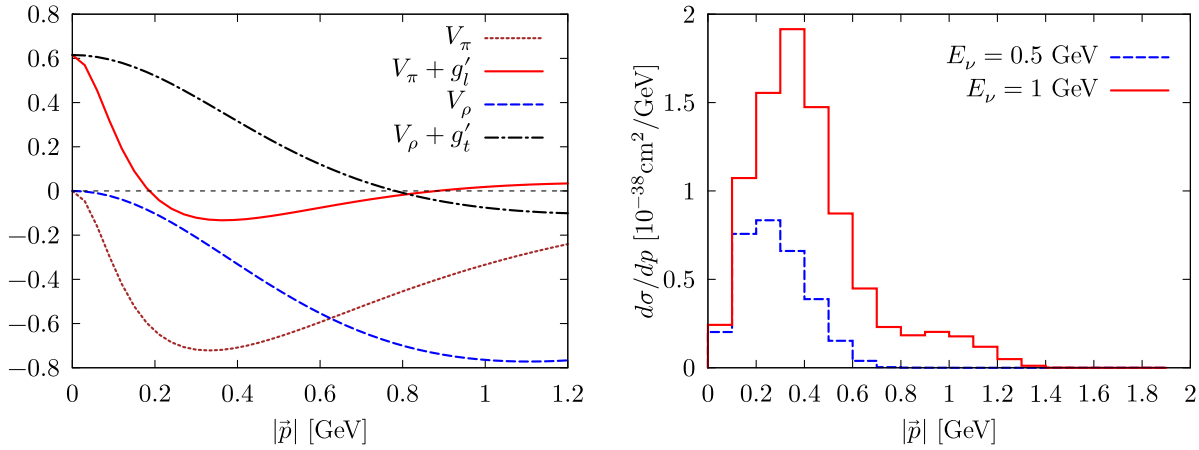

FIG. 5. Left panel: Longitudinal and transverse channels of in-medium $\sigma\sigma\tau\tau$ potential $V(p)$ in the static limit $p^0 = 0$ given in $[m_\pi^{-2}]$. Solid red and dotted-dashed black lines correspond to the final interactions, with the addition of the g_l' and g_t' terms. Right panel: Monte Carlo distribution of momentum exchanged between two ph-ph excitations in the calculation of the 2p2h reaction mechanism for incoming neutrino energies of 0.5 and 1 GeV.

introduced, fulfilling the conditions:

$$\Omega(\vec{r} = \vec{0}\,) = 0\,, \qquad \Omega(\vec{r}\,) \approxeq 1 \text{ for } |\vec{r}\,| \gtrapprox r_c, \tag{12}$$

with r_c a distance between nucleons below which they feel a strong repulsion whose details cannot be disentangle in the medium. The distance r_c is estimated to be around 2.6 fm, which corresponds to the mass of the ω meson, $q_c =$ 780 MeV. The desired behavior of the potential is imposed by modulating the potential with the short-distance function,

$$V(\vec{r}\,) = [V_\pi(\vec{r}\,) + V_\rho(\vec{r}\,)]\,\Omega(\vec{r}\,). \tag{13}$$

The functional form of $\Omega(\vec{r}\,)$ is taken to be $[1 - j_0(q_c|\vec{r}\,|)]$ (spherical Bessel function) whose Fourier transform reads:

$$\Omega(\vec{k}) = (2\pi)^3\delta^3(\vec{k}) - \frac{2\pi^2}{q_c^2}\delta(|\vec{k}| - q_c). \tag{14}$$

With all these elements we can write the potential in momentum space as:

$$\begin{aligned} V(p) &= \int \frac{d^3k}{(2\pi)^3}[V_\pi(p_0, \vec{p} - \vec{k}) + V_\rho(p_0, \vec{p} - \vec{k})]\Omega(\vec{k}) \\ &= V_\pi(p) + V_\rho(p) \\ &\quad - \int \frac{d^2\hat{k}}{4\pi}[V_\pi(p_0, \vec{p} - q_c\hat{k}) + V_\rho(p_0, \vec{p} - q_c\hat{k})]. \end{aligned} \tag{15}$$

After performing the integration, averaging over angles, we finally obtain [11]:

$$\begin{aligned} g_l'(p) &= -\left(\vec{p}^{\,2} + \frac{1}{3}\,q_c^2\right)\tilde{F}_\pi^2\,\tilde{D}_\pi - \frac{2}{3}C_\rho\,q_c^2\,\tilde{F}_\rho^2\,\tilde{D}_\rho, \\ g_t'(p) &= -\frac{1}{3}\,q_c^2\,\tilde{F}_\pi^2\,\tilde{D}_\pi - \left(\vec{p}^{\,2} + \frac{2}{3}q_c^2\right)C_\rho\,\tilde{F}_\rho^2\,\tilde{D}_\rho, \end{aligned} \tag{16}$$

where $\tilde{F}_{\pi,\rho}$ and $\tilde{D}_{\pi,\rho}$ correspond to form factors and propagators with shifted momentum $\vec{p}^{\,2} \to \vec{p}^{\,2} + q_c^2$. In the left panel of Fig. 5 we show the effect of g_l' and g_t' on the potential. Let us notice that in the limit of high-momentum transfer $|\vec{p}\,| \gg q_c$, the potential goes to 0, while in the regime of low-momentum transfers we obtain $g_l' = g_t' = 0.63$. This is a value we used in previous calculations of the RPA [45,48] and 2p2h excitation [18] effects on CCQE reactions. In the right panel of Fig. 5 we show the region of $|\vec{p}\,|$ (exchanged momentum between two ph-ph excitations) probed in the calculation of 2p2h contribution. For both neutrino energies, $E_\nu = 0.5$ GeV and $E_\nu = 1$ GeV, the momentum distributions peak at rather low values (0.2 and 0.4 GeV, respectively). In this region the contribution coming from the longitudinal part of interaction $V_l(p) = V_\pi(p) + g_l'(p)$ is relatively small in comparison to the transverse one (see the left panel of Fig. 5). The short-distance g_l' term largely interferes with the pion-exchange potential, giving rise to an interaction significantly different than V_π. The former term modifies the low-energy region but also cancels out the high-energy contribution that would otherwise emerge from one-pion exchange. On the other hand, the ρ propagator is largely suppressed by m_ρ, but the transverse interaction gets enhanced due to g_t'. Ultimately, the strength is dominated by the transverse channel, shown in Fig. 5 by the dotted-dashed black line.

An analogous discussion to that above holds in the case of Δh-Δh and ph-Δh effective interaction in the nuclear medium, with appropriate spin and isospin operators $\vec{\sigma} \to \vec{S}$ and $\vec{\tau} \to \vec{T}$ and replacing the coupling constant $f_{\pi NN}$ by $f^*_{\pi N\Delta}$ $(= \sqrt{4\pi \times 0.36})$. In addition, C_ρ and the form factors F_π, F_ρ are the same for both nucleon and $\Delta(1232)$ cases [11,47].

Finally, the in-medium interaction is obtained after performing some resummations, in the RPA sense and driven by the effective NN, $N\Delta(1232)$, and $\Delta\Delta$ potentials. Hence, it includes both short- and long- (RPA) range correlations. Full details can be found in Refs. [18,25,38].

C. Treatment of $\Delta(1232)$

We briefly sketch here the steps given in Ref. [18] to calculate the inclusive 2p2h cross section:

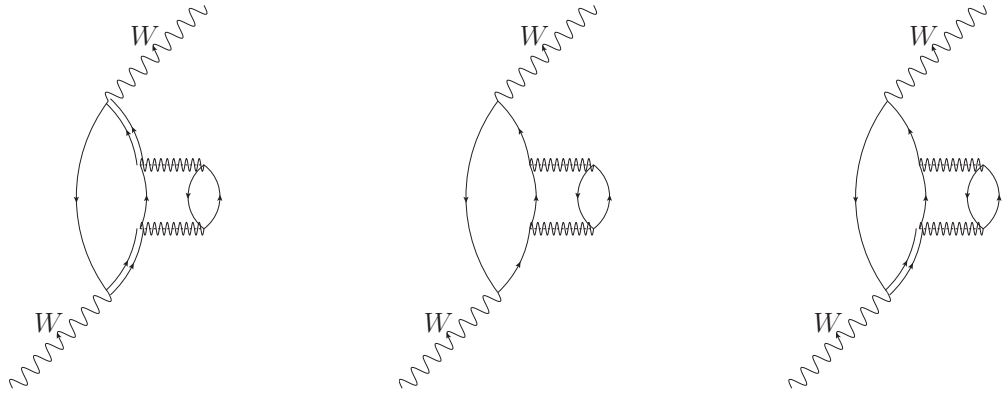

FIG. 6. Three different contributions to the 2p2h hadron tensor. In the left plot the diagram has two direct $W^+\Delta N$ vertices (and two Δ propagators) and it can be cast as Δh excitation, with a self-energy insertion for the resonance. We will refer to it as the "$\Delta\Delta$ diagram." In the middle, the diagram contains two direct W^+NN vertices, and it builds an in-medium nucleon self-energy. In the right plot an interference term is shown with both $W^+\Delta N$ and W^+NN vertices (one Δ and another nucleon propagators), referred to as the "$N\Delta$ diagram." In all the cases the second ph is excited either from the longitudinal or transverse spin-isospin interaction.

(i) Performing the full calculation of diagrams implicit in Fig. 1, replacing the pion and ρ exchanges with the effective spin-isospin interaction both in the longitudinal and transverse channels. Next, the contributions which have two direct $W^+N\Delta$ vertices (we will denote them as $\Delta\Delta$ diagrams, see the left panel of Fig. 6) or two W^+NN vertices (the central panel of Fig. 6) for both longitudinal and transverse channels are subtracted from the full sum. The latter diagrams, driven by the longitudinal and transverse spin-isospin interactions, are removed because they give contribution to the nucleon spectral function and thus should be taken into account when the QE mechanism is considered. In turn, the $\Delta\Delta$ diagrams can be seen as Δh nuclear excitation, with resonance dressed in the nuclear medium.

(i) Computing the Δh excitation by the W boson, including the imaginary part of the Δ self-energy, which accounts for the 2p2h and 3p3h contributions to the Δ self-energy, Σ_Δ, as calculated in Ref. [11]. There are also some pion production quasielastic contributions included to $\mathrm{Im}\Sigma_\Delta$, which, however, do not lead to multinucleon absorption in first approximation. Note that in addition in Ref. [18], $\mathrm{Re}\Sigma_\Delta$ is set to zero since its inclusion would require a detailed RPA resummation, with separate longitudinal and transverse series.

To find the predictions of the model of Ref. [18] for exclusive observables (such as outgoing nucleons momenta), we encounter a fundamental obstacle in the aforementioned procedure. The $\mathrm{Im}\Sigma_\Delta$, which gives a major contribution to the total 2p2h cross section, is parametrized in Ref. [11] in terms of the kinetic energy of a pion that would excite a Δ with the corresponding invariant mass. The information about underlying dynamics of excited nucleons is already integrated out. To overcome this problem, we have explicitly evaluated here the $\Delta\Delta$ contribution (the first diagram of Fig. 6), instead of using the precomputed $\mathrm{Im}\Sigma_\Delta$ with the appropriate C_{A_2} parameter (see Eq. (51) of Ref. [18]). We have followed the original calculation of the Δ self-energy carried out in Ref. [11] where $g'_l(p) \neq g'_t(p) \neq g'$, as explained in the previous subsection. The energy dependence of g'_l and g'_t parameters will affect especially high-energy transfers regime where particularly g'_l differs considerably from the constant $g' = 0.63$.

D. Further refinements of Δ

Following the results presented in Ref. [22], we will introduce two modifications to the treatment of Δ excitation which were proposed to achieve a better agreement with the neutrino Argonne National Laboratory (ANL) and Brookhaven National Laboratory (BNL) data in the $\nu_\mu n \to \mu^- n\pi^+$ channel. First, we will employ a C_A^5 form factor for the Δ-N electroweak transition given by

$$C_A^5(q^2) = \frac{1.18}{\left(1 - q^2/M_{A\Delta}^2\right)^2}, \quad M_{A\Delta} = 950\ \mathrm{MeV}. \tag{17}$$

Second, we change the Δ propagator from the Rarita-Schwinger form to the pure spin-3/2 projector operator, including a p_Δ^2/M_Δ^2 local factor which is equal to 1 at the Δ peak,

$$\begin{aligned} G_{\mu\nu}(p_\Delta) &= \frac{p_\Delta^2}{M_\Delta^2}\frac{P^{\frac{3}{2}}_{\mu\nu}(p_\Delta)}{p_\Delta^2 - M_\Delta^2 + iM_\Delta\Gamma_\Delta} \\ P^{\frac{3}{2}}_{\mu\nu}(p_\Delta) &= -(\not{p}_\Delta + M_\Delta)\Big[g_{\mu\nu} - \frac{1}{3}\gamma_\mu\gamma_\nu \\ &\quad - \frac{1}{3p_\Delta^2}(\not{p}_\Delta\gamma_\mu p_{\Delta\nu} + p_{\Delta\mu}\gamma_\nu\not{p}_\Delta)\Big]. \end{aligned} \tag{18}$$

This corresponds to the prescription of using consistent Δ couplings [49]; however, it does not precisely recover the results of Ref. [22], where a 1/2-spin part of Δ propagator was partially retained. We have checked, though, that the difference is small and in our calculation can be safely neglected.

Furthermore, the neglect of the spin 1/2 degrees of freedom and the use of consistent vertices lead to an accurate reproduction of the Watson's unitary theorem in the dominant P_{33} multipole [50], without including any further sizable phase [22].

E. 3p3h

The new treatment of the $\Delta\Delta$ diagram, as exposed in Sec. II C, enables us to calculate the distribution of outgoing nucleons for the two-body reaction mechanism associated to this diagram. In the former works [2,18], the imaginary part of the Δ self-energy was composed of four contributions (Pauli blocking, 1p1h1π, 2p2h, and 3p3h) of which the latter two were included to account for the multinucleon knockout inclusive cross section. Presently, the MC generators which use this model usually follow this prescription. This approximation is reasonable since we suspect that for three outgoing nucleons the least-energetic one will hardly ever be detected due to the experimental energetic threshold.

In the following, we will treat separately the 2p2h and 3p3h contributions, since we are interested in the dynamics of the outgoing nucleons. The only 3p3h source in the model comes from the corresponding mechanism included in $\mathrm{Im}\Sigma_\Delta$ in the $\Delta\Delta$ diagram. However, we have many other sources of two body absorption besides the latter diagram, some of them not involving the excitation of the Δ resonance. For the time being, we use a parametrization of the 3p3h process reported in Ref. [11] where it is given as a function of the kinetic energy of a pion that would excite a Δ with the corresponding invariant mass. The calculation of the final states in the 3p3h process is a nontrivial task and goes beyond the scope of the present analysis.

III. CALCULATION IN NEUT

In NEUT [21], the events are generated according to the distribution of the outgoing lepton, i.e., using the weight given by the value of double-differential inclusive cross section, expressed as the contraction of lepton and hadron tensors as given by Eq. (2). The hadron tensor $W^{\mu\nu}$ is evaluated following Ref. [18]. It is computed separately for proton-neutron and proton-proton final states and used to provide isospin-dependent final states. The location of the interaction vertex in the nucleus is chosen according to the density profile and the initial-state nucleons are picked below the Fermi level corresponding to the radial position following the local Fermi gas model recipe. The outgoing nucleons at the weak vertex are distributed according to the available phase space. They are generated uniformly in the center of the mass of the hadronic system and boosted to the laboratory rest frame. Next, their momenta are tested against the local Fermi level to implement Pauli blocking. This procedure neglects the dynamics of underlying nuclear model and produces a symmetric distribution of outgoing nucleons. The produced pair of nucleons is fed into the NEUT cascade model accounting for the transport of nucleons in the high-density nuclear medium. The model of the NEUT cascade is based on the model developed in Ref. [51] modified by the experimental nucleon-nucleon and pion-nucleon cross-section data when available [52].

The same cascade model is used to calculate the final-state nuclear reinteraction migration matrices that are used to estimate the effects on the new 2p2h hadron kinematics predictions. These migration matrices describe the transport of the particles from the interaction point to the outside of the nucleus one by one and considering the momentum and nature of the particles. These matrices are used later to compute the visible final energy outside of the nucleus, see the results of Sec. IV B.

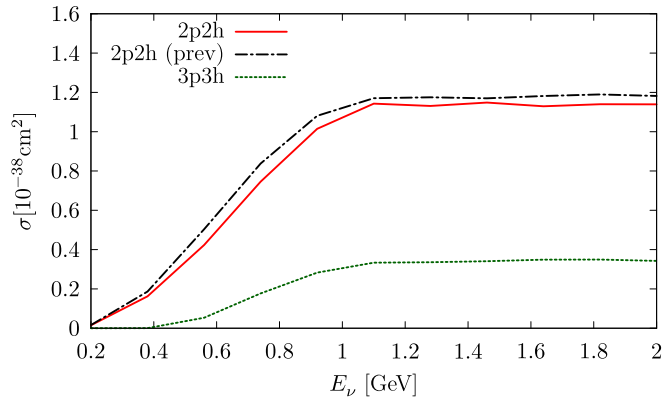

FIG. 7. Total cross section σ $[10^{-38}\mathrm{cm}^2]$ on ^{12}C as a function of incoming neutrino energy E_ν. The solid red and dashed-dotted black curves correspond to two calculations of the 2p2h explained in the text. The difference between both cross sections can be understood as a theoretical uncertainty of our approach. The dotted green curve corresponds to 3p3h and should be added to the 2p2h contribution. In all cases, the cut $|\vec{q}| < 1.2$ GeV in the momentum transfer is applied.

IV. RESULTS

As we have stated in Sec. II E, in the following analysis we will treat separately the 3p3h contribution to the Δ self-energy, while the NEUT results are shown with both 2p2h and 3p3h inclusions according to the current model implementation.

A. Total cross-section and lepton differential distributions

In Fig. 7 we show the total cross section for both 2p2h and 3p3h mechanisms on ^{12}C. With the solid red line we plot the result obtained with the present calculation. The dashed-dotted black line labeled "2p2h (prev)" corresponds to the 2p2h result in which we include $\mathrm{Im}\Sigma_\Delta$ as in Ref. [18].[5] We interpret the difference between the two calculations as a theoretical uncertainty of our approach, which is at the order of 5–10%. In the latter one, the 2p2h inclusion into the Δ self-energy was parametrized (thus introducing some approximations). The 3p3h contribution, calculated according to Ref. [11], is shown by the green dotted line. It corresponds to around 20% of the total 2p2h cross section for neutrino energies above 1 GeV. This prediction should be treated with some caution. In principle a more careful 3p3h calculation could be performed but, as mentioned, it is technically complicated and the smallness of the expected differences discourage

[5]It means that we do not follow modifications described in Sec. II C to compute the Δ-Δ contribution; however, we do introduce the refinements described in Secs. II B and II D.

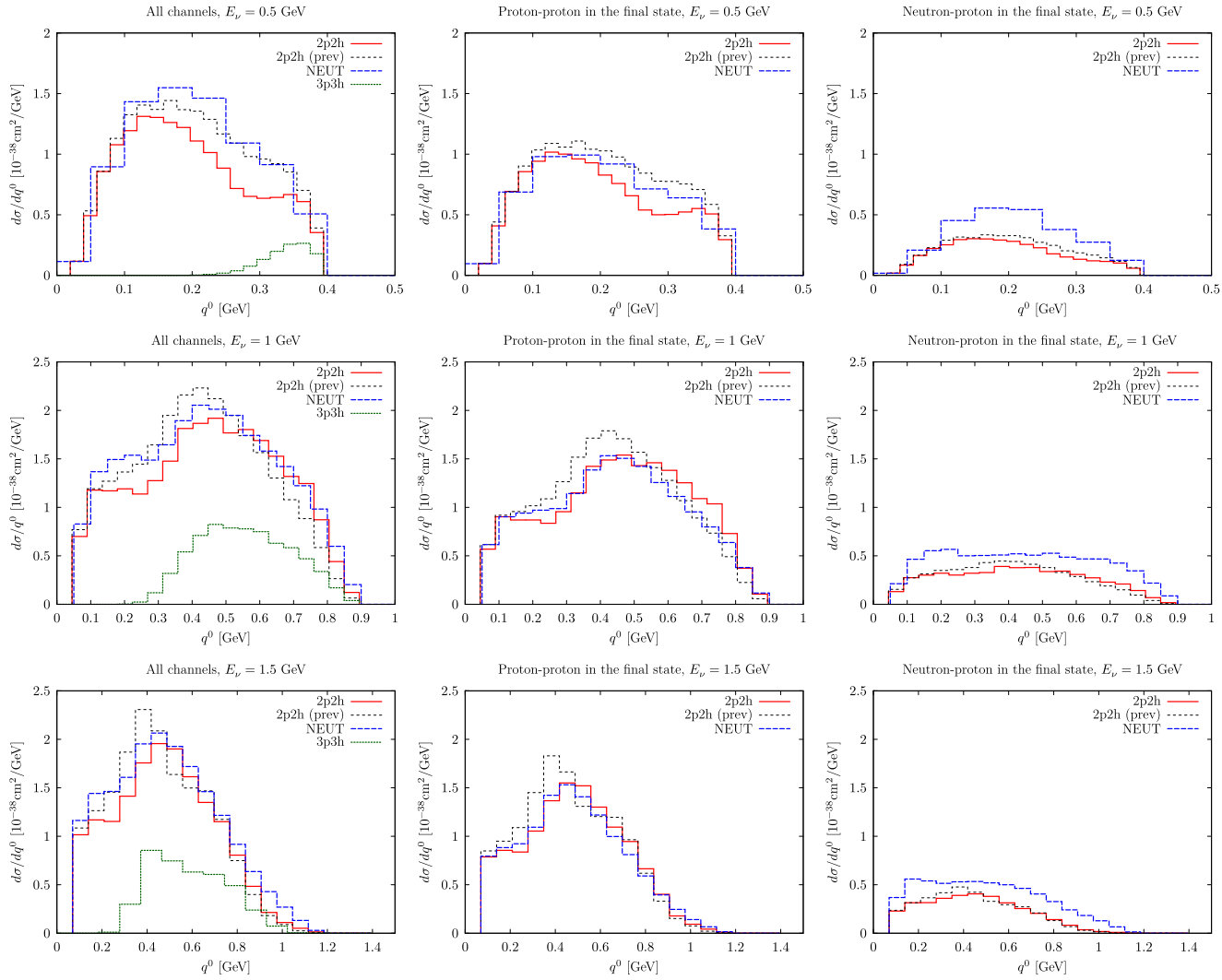

FIG. 8. $d\sigma/dq^0$ differential cross section on ^{12}C for three different incoming neutrino energies: $E_\nu = 0.5$, 1, and 1.5 GeV, displayed in the top, middle, and bottom rows, respectively. Results in the left column are summed over isospin, while the central (right) column corresponds to two protons (one neutron and one proton) in the final state. In all cases, the cut $|\vec{q}| < 1.2$ GeV in the momentum transfer is applied.

for the time being from further inquiries. Still, the approach we follow is one of the very few existing and the most widely used in the studies of neutrino-induced reactions.

All the curves in Fig. 7 have a similar energy dependence, with a plateau above $E_\nu \approx 1.1$ GeV. The reason for this behavior is a cut we impose in the momentum transfer $|\vec{q}| < 1.2$ GeV, which affects largely the cross section for $E_\nu > 1$ GeV. Thus, for instance, for $E_\nu = 1.5$ GeV this cut is responsible for neglecting around 10% of the available phase space. Our model cannot probe high-energy-momentum transfers for various reasons. First, the nonresonant terms of $W^\pm \pi N$ vertex are obtained within the chiral perturbation theory and can be safely used only for low- and moderate-energy-momentum transfers. Besides, we do not include higher resonances above Δ exchange. Moreover, our model for effective in-medium interactions was constructed to describe exchange of moderate momenta between ph or Δh excitations. This momentum transfer sharp-cutoff corrects for the growth of the 2p2h+3p3h cross section with the neutrino energy, for $E_\nu > 1.2$ GeV, found in the previous results of Ref. [18] (see, for instance, green squares in Fig. 5 of Ref. [2]). Below, $E_\nu < 1.2$ GeV, we successfully reobtain the bulk of the results already published. There exist minor differences that can be ascribed to the new treatment of the Δ. We will see below that this is also the case for the outgoing lepton differential distributions.

In Figs. 8 and 9 we show the $d\sigma/dq^0$ and $d\sigma/d\theta_\mu$ lepton differential cross sections, respectively, for three incoming neutrino energies, $E_\nu = 0.5,\ 1,\ 1.5$ GeV (rows) and for three cases of the isospin state of final nucleons: summed over isospin states (left), for two protons (middle), or for neutron-proton final state (right). The dashed blue line corresponds to the NEUT result, which follows the approach of Ref. [18] (we note that in this case the 3p3h contribution is included). For the $d\sigma/dq^0$ distribution at $E_\nu = 1$ GeV (the middle row in Fig. 8) we can clearly observe two peaks, at $q^0 \simeq 0.15$ GeV and $q^0 \simeq 0.45$ GeV, for the NEUT and for the 2p2h distributions. They correspond to two distinct dynamical

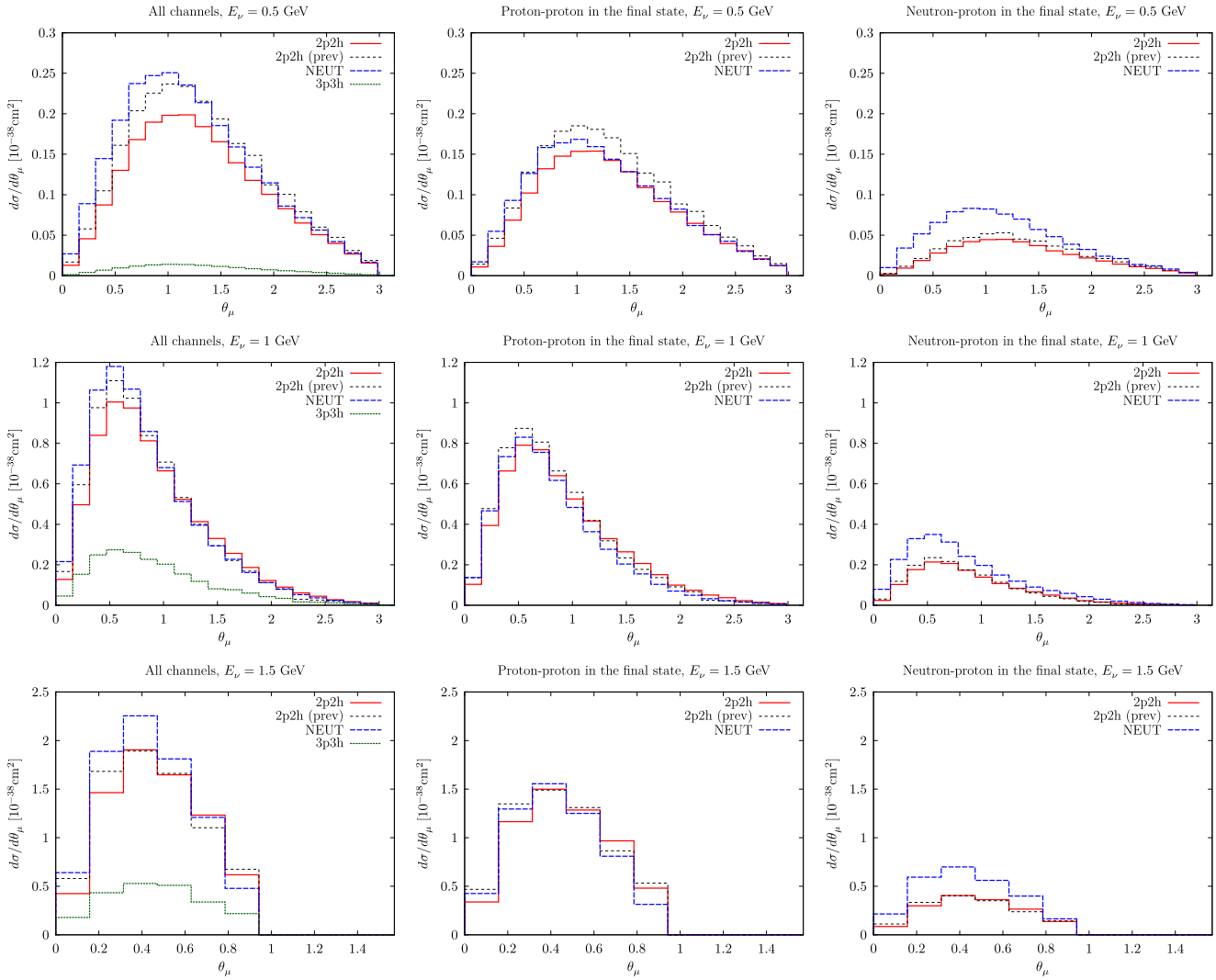

FIG. 9. As in Fig. 8 but for $d\sigma/d\theta_\mu$ differential cross section.

mechanisms which dominate the total cross section. The first one (which peaks at lower-energy transfers) is the contribution driven by the interference $N\Delta$ diagram (see the last plot in Fig. 6). The second one comes from the $\Delta\Delta$ diagram (first one in Fig. 6). Their relative position can be understood since a Δ resonance has a mass around 0.3 GeV higher than a nucleon and therefore the $N\Delta$ and $\Delta\Delta$ diagrams produce peaks which are around 0.3 GeV apart. Consequently, the theoretical uncertainty of our approach affects mostly the region of the second peak since it is driven by the treatment of 2p2h inclusion to $\mathrm{Im}\Sigma_\Delta$. This can be observed in all the panels of Fig. 8 where this peak is slightly lower and shifted toward higher-energy transfers when comparing the "2p2h" to "2p2h (prev)" results. The total 3p3h strength for each considered energy is consistent with the results of Fig. 7, and it is almost negligible for $E_\nu = 0.5$ GeV and then grows to $E_\nu \approx 1.1$ GeV, when it stabilizes thanks to the implementation of the cutoff in the transferred momentum. The 3p3h $d\sigma/dq^0$ distribution is shifted toward high-energy transfers where larger phase space is available and, thus, three particles can be produced ore easily. This contribution has been calculated and parametrized in such a way that there is no direct way to split it into various isospin channels.

The panels in the middle column in Figs. 8 and 9 show distributions for two protons in the final state. They clearly dominate over the process in which a neutron-proton pair is produced, as shown in the right column. We should point out that NEUT leads to much higher cross sections for the np pair. In principle in the region of high-energy transfers, where the $\Delta\Delta$ diagram dominates, the proportion of pp to np should be in the ratio five to one [18,53]. However, such pattern is not followed by the NEUT sample. The difference might be partially due to the implementation of the 3p3h contribution within NEUT.

In all the panels of Figs. 8 and 9 we observe some differences between the NEUT results and the two predictions for the 2p2h. Nevertheless the agreement is sufficiently fair to confirm the reliability of the two-nucleon absorption neutrino cross sections previously published [18] and widely used by the neutrino community. There are three reasons responsible for the existing discrepancies: (i) the contribution of 3p3h is only included in the NEUT calculation, (ii) the change of

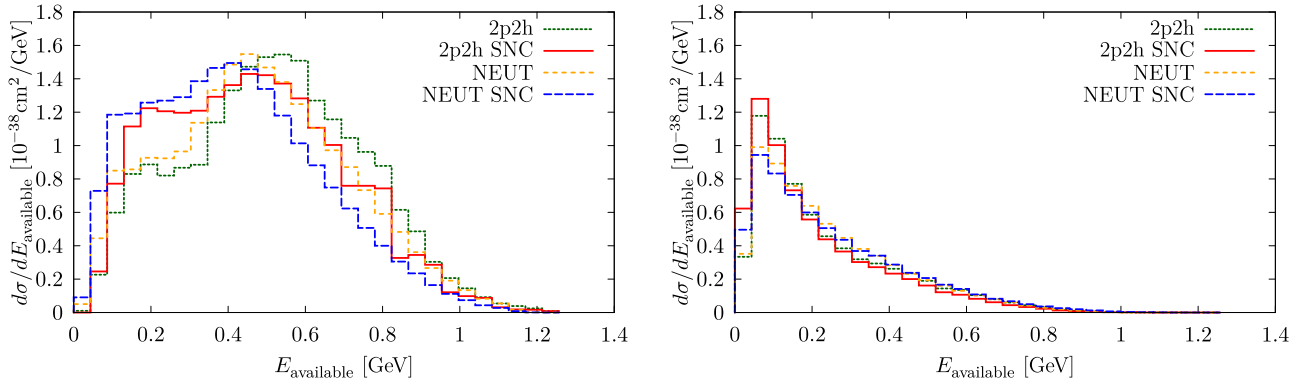

FIG. 10. Available energy for $E_\nu = 1.5$ GeV. Left: Results for two protons produced in the primary vertex. Right: Results for proton-neutron final state in the primary vertex. Curves denoted as "SNC" were obtained with the migration matrices generated with the NEUT Monte Carlo event generator.

g' to $g'_l(p)$ and $g'_t(p)$ of the Δ propagator and the C_A^5 form factor, and (iii) the abandonment of the use of any averaged nucleon momentum in the computation of the hadron tensor. The change of g' from a constant to a momentum-energy-dependent function influences predominantly the contribution coming from the $\Delta\Delta$ and $N\Delta$ diagrams (see the left and the right panels of Fig. 6). Other changes enlisted in (ii) and (iii) do not have a large impact on the final result. In fact, partially they even compensate, since (iii) tends to lower the cross sections, while the new value of C_A^5 produces a certain enhancement.

B. Available energy

In several neutrino oscillation experiments the neutrino energy is reconstructed using a calorimetric approach, i.e., by measuring the energy deposited by the outgoing hadrons simultaneously detecting the final lepton. For this kind of analysis (e.g., performed by the MINERvA experiment [54]) the concept of available energy is used, as an attempt to reconstruct the total hadronic energy. For this comparison, we estimate the available energy as the sum of the kinetic energy of all the protons leaving the nucleus.

The MINERvA results [54] point out to a deficit of events with two nucleons in the final state in the predictions obtained from the implementation of theoretical model derived in Ref. [18], within the GENIE Monte Carlo event generator. The 1p1h and 2p2h models used in this Monte Carlo generator are similar to the ones implemented in NEUT. The purpose of this section is to identify whether and how a more accurate description of the final state affects the prediction of the available energy.

When a neutron-proton pair is produced, the visible energy strongly depends on how the energy is distributed between the two nucleons. In turn, when two protons are produced, in first approximation, the total energy of the final state should be just a function of the energy transferred to the final-state hadrons, and thus it should not depend on how the energy is shared between the two final protons. This statement might not be totally correct and can be altered by the final-state transport of the nucleons through the nucleus. This is because the intranuclear cascade depends on the kinetic energy of the traveling nucleons. It is therefore critical to convolute the predictions of the model for the first step (primary reaction) with a reasonable description of the nucleon transport in the nucleus, accounting for secondary collisions. To perform this calculation we used migration matrices, generated by the NEUT's cascade, which transform the neutron and proton kinetic energies obtained at the primary vertex into the distribution of energy of outgoing protons after the internuclear cascade. Nucleons suffer mostly elastic scatterings, which cause a smearing of the kinetic energy. Only a small ratio of neutrons transform into protons. Note that these latter effects were not considered in the previous Figs. 8 and 9.

Using the NEUT migration matrices, we obtain the energy distribution of the outgoing protons after the cascade or, equivalently, the available energy. In Fig. 10 we show such a distribution both for NEUT and for our present calculation for $E_\nu = 1.5$ GeV. In the left panel we show the situation for two protons in the final state. The difference in normalization comes from the differences between NEUT and present calculation mentioned before. Nevertheless, we observe very similar shapes of the distributions. This should not be surprising for the primary vertex, since—as mentioned—the total kinetic energy of the outgoing protons depends on the energy transferred to the nucleus and not on the details of how the energy is distributed between the two outgoing nucleons. The cascade smears the two-peak structure (whose origin we have already attributed to two dynamical mechanisms represented by the $N\Delta$ and $\Delta\Delta$ diagrams) and shifts strength toward lower energies.

The right panel of Fig. 10 corresponds to the neutron-proton final state. In all the cases the distribution peaks at around 0.075 GeV (corresponding to a proton with a momentum of approximately 375 MeV). We do not observe the characteristic two-peak structure and the effect of the intranuclear cascade is milder than for the proton-proton final state. Still, the difference between the two approaches is well visible. Apart from the normalization factor, the tail of the distribution is much steeper for the "2p2h" predictions. This behavior can be better understood when we look at the two-dimensional momentum distributions of the final nucleons, presented in the next subsection.

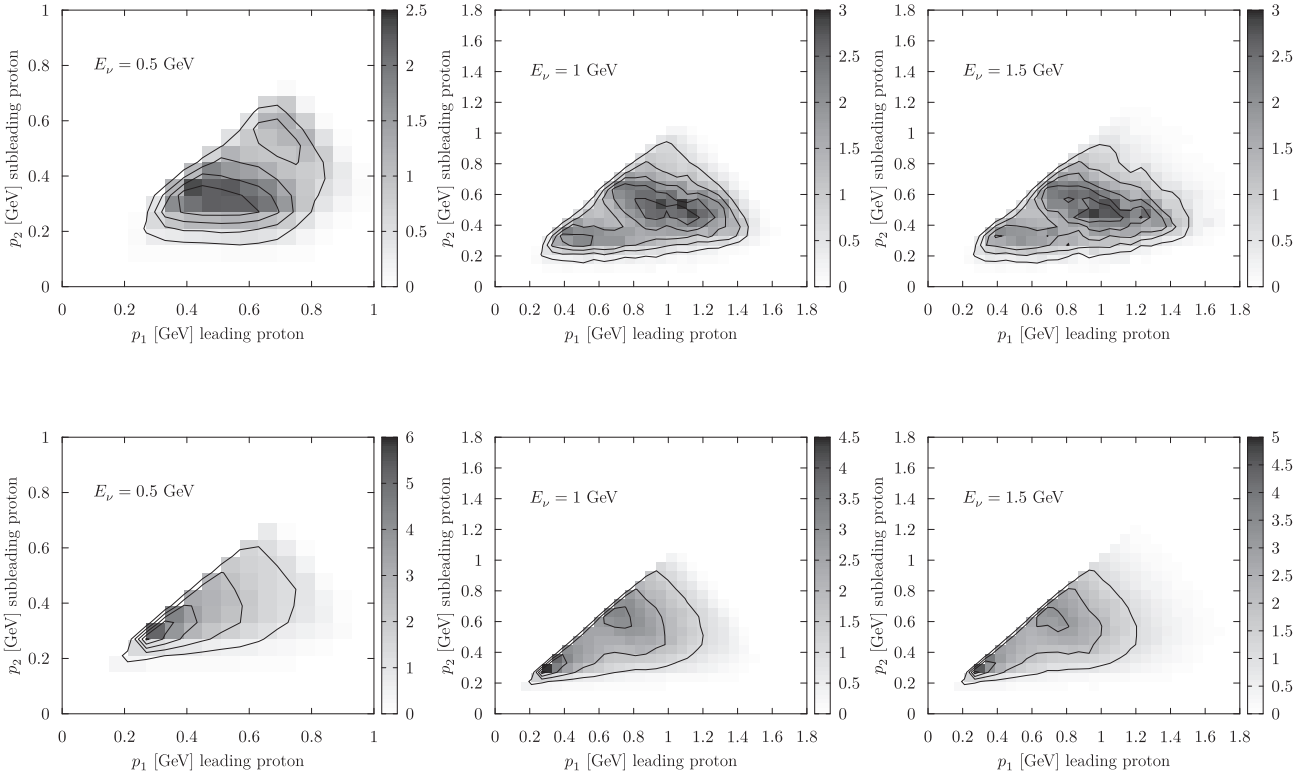

FIG. 11. Outgoing nucleons distribution $d\sigma/d|\vec{p}_1|d|\vec{p}_2|$ (10^{-38} cm^2/GeV^2) for two protons in the final state. The momentum $|\vec{p}_1|$ corresponds to higher energetic (leading) proton, while $|\vec{p}_2|$ to the subleading one. The panels from the left to right are for incoming neutrino energies of $E_\nu = 0.5$, 1, and 1.5 GeV, respectively. In all cases, the target nucleus is ^{12}C. Upper panels show the results for the "2p2h" model, while the bottom ones have been obtained using NEUT.

C. Outgoing nucleons distribution

When considering the $d\sigma/\, d|\vec{p}_1|d|\vec{p}_2|$ distribution of two nucleons in the final state, we will focus on the primary vertex of interactions and analyze separately the proton-proton and neutron-proton cases. In the latter situation the particles are distinguishable, while for two protons, we will look at the distribution of higher- versus lower-energetic proton. This cross section is shown in Fig. 11. In the upper panels the results of our current "2p2h" calculation are presented. They differ substantially from the distributions provided by NEUT, displayed in the bottom panels. The NEUT results are symmetric (let us point out that the scale used in the bottom panels is around twice larger than for the upper ones). For $E_\nu = 1$, 1.5 GeV we observe two dominating peaks of the distributions. The first one—which is also present for the $E_\nu = 0.5$ GeV case—corresponds to the momenta of $p_1 \approx$ 0.4–0.5 GeV, $p_2 \approx 0.3$–0.4 GeV (upper panels) and $p_1 \simeq p_2 \simeq 0.3$ GeV (lower panels). This peak is generated by the $N\Delta$ diagram (see the right panel Fig. 6). Another, much wider, peak is visible for $p_1 \approx 0.9$–1.2 GeV, $p_2 \approx 0.4$–0.5 GeV ("2p2h" results in the upper panels) and for $p_1 \simeq p_2 \simeq 0.7$ GeV (NEUT results), generated by the $\Delta\Delta$ diagram. It is worth noting that the current "2p2h" results predict a much higher rate of energetic nucleons in comparison to NEUT. This observation might influence the experimental analysis since the number of observed protons depends on the detector threshold. It might happen that when the energy is distributed equally between two protons (like it is done in NEUT) they both would lie below the detection threshold and no signal would be predicted. In this case, the asymmetric energy distribution favours the detection of the more energetic one.

For the case of neutron-proton final state, the cross section is much lower than in the proton-proton case. In Fig. 12 we show results for $E_\nu = 0.5$, 1, and 1.5 GeV. We observe that the distribution is symmetric for the NEUT (bottom panels), as it follows directly from the procedure of how the nucleons' momenta are generated. Our model predicts a quite different distribution although much more symmetric than in the case of proton-proton production. This shape can be understood when we realize that there are two main contributions to the cross section. The interaction on the initial neutron-neutron pair may produce a proton in the ph excitation directly connected to the W^+ boson. In this case, a much higher energy momentum is transferred to the proton. Inversely, when a neutron is produced in the leading ph, it becomes much more energetic. These two possible contributions have similar strengths (which can be also inferred when analyzing the Clebsh-Gordan coefficients of both channels). When they are summed, the resulting "L" shape is obtained, clearly visible in the upper panels of Fig. 12.

V. CONCLUSIONS AND OUTLOOK

We have presented a revised calculation of 2p2h mechanism induced by CC neutrino scattering, following the theoretical approach of Ref. [18], and confirmed the reliability

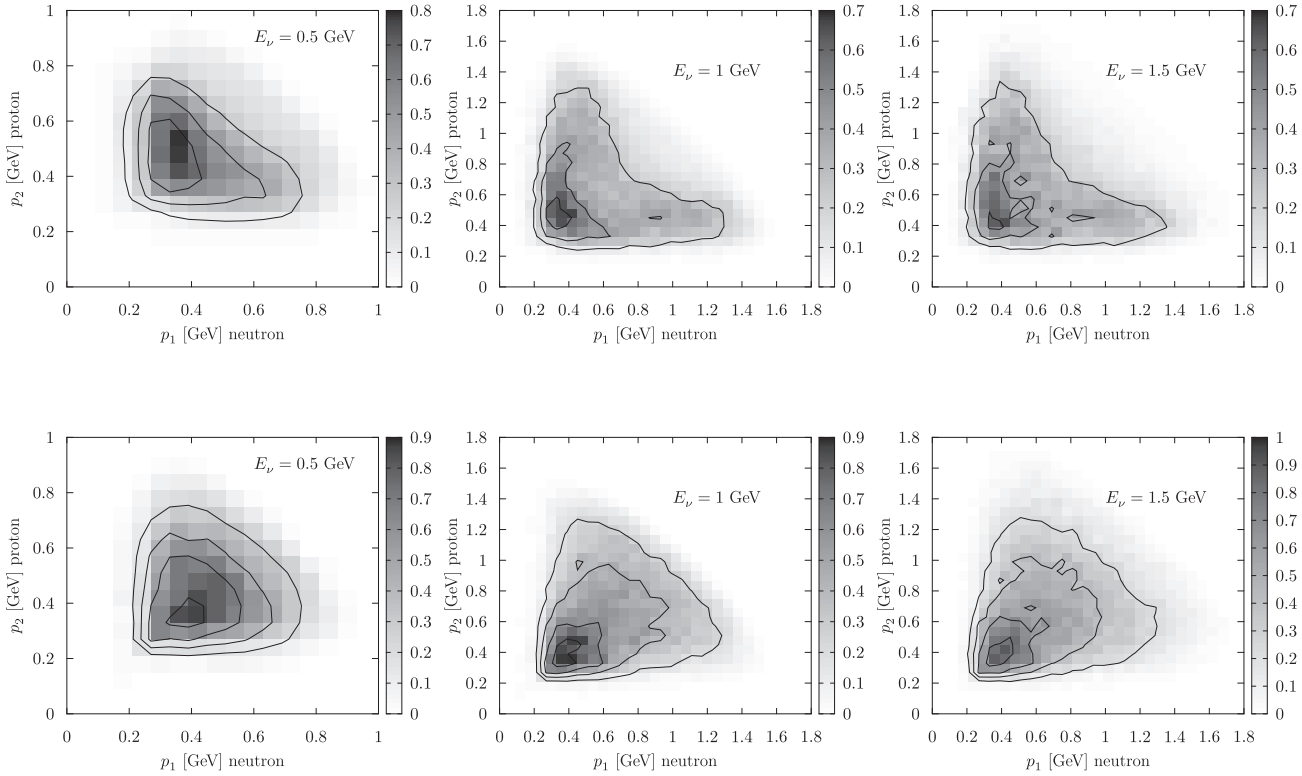

FIG. 12. Outgoing nucleons distribution $d\sigma/\, d|\vec{p}_1|d|\vec{p}_2|$ (10^{-38} cm^2/GeV^2) in the case of neutron-proton pair produced in the final state. The panels from the left to right correspond to incoming neutrino energy $E_\nu = 0.5$, 1, and 1.5 GeV on ^{12}C. Upper panels show the results for the "2p2h" model, while the bottom ones for NEUT.

of previous results, widely used by the neutrino cross-section community.

In this work we lifted some of the approximations used previously. In particular, the momentum and energy dependence of g'_l and g'_t parameters of the effective in-medium nucleon-nucleon potential has been retained. This allowed us to calculate directly the inclusion of the $\Delta\Delta$ diagrams which beforehand were added using a parametrized result from Ref. [11]. Also, we have updated the way how the Δ propagator is treated, retaining only the spin-3/2 part using consistent couplings, and we have included the most recent value of the C_A^5 form factor fitted to the available electroweak pion production ANL and BNL data. The difference between our current and previous calculations can be treated as a theoretical error of our approach. An overall uncertainty in the total cross section does not exceed 10%.

Although the distributions of the outgoing leptons are not much affected by the introduced changes, the experimental analyses usually depend also on other observables and details of theoretical models. This motivated our further inquiries into the hadronic final states. With the NEUT migration matrices we were able combine our model predictions in the primary vertex of interaction with realistic estimates of the intranuclear cascade effects.

We also separated the 2p2h and 3p3h contributions and consequently—with the above mentioned updates—we gained an insight into the distribution of outgoing nucleons, considering different isospin channels. We have compared the outgoing nucleons' momentum distributions, coming directly from our microscopic approach, with the ones obtained within NEUT, where the nucleons generated isotropically in the hadronic center of mass according to the available phase space. The procedure followed by NEUT is implemented in other Monte Carlo event generators, so the results of our analysis can be directly applied also to them.

In the case of proton-proton final state, we predict a strong asymmetric signal with one of the protons more energetic than another. For the neutron-proton case, the obtained distribution is also quite different from the isotropic result. How these predictions would enter and alter the existing experimental analyses depends on the used detection techniques. Certainly, some differences should be visible due to the proton's momentum thresholds. Also, it has been often argued that the information about exclusive hadronic states in the neutrino-nucleus scattering is an important observable which can help to discern between various theoretical approaches.

According to our predictions, the 3p3h contribution is important and might even amount to 20% of the 2p2h strength for energy-momentum transfer regions. It would therefore be interesting and useful to redo the calculation of Ref. [11], in the same way as we did for the 2p2h, to get further insight into the strength coming from different isospin channels of this process. The transferred energy this time would be divided into three outgoing nucleons, thus making them on average less energetic (and more difficult to observe because of the detector's threshold). We suspect that—the same way as in the 2p2h case—the momentum distribution of the outgoing particles would be asymmetric with one leading nucleon.

Further analysis of multinucleon knockout cross sections for antineutrino-induced and neutral-current driven processes are natural continuation of the present work and we are already working on them. Available antineutrino-nucleus scattering data are less accurate due to lower event rate (and therefore higher statistical uncertainties), leading to weaker constraints for theoretical models. Still, this channel will play a crucial role in the experimental programs aiming at measuring the CP-violating phase. The NC 2p2h is a less explored channel due to the experimental difficulty of performing a measurement. However, it should also be included in the Monte Carlo generators, treating it as a background process. An analysis of how its presence affects the experimental studies is hence a important topic for future work.

We conclude by noting the discussion we have had about the adopted framework in a broader context, describing to what extent nuclear correlations are included. We have seen that 2p2h many-body diagrams involving ISC are of higher order, within the underlying density expansion assumed in the model and that have been neglected. The systematic inclusion of such contributions is not straightforward due to the presence of effective parameters adjusted to data in the past. In fact, their phenomenological values could account partially for neglected higher-order corrections, as it occurs in any counting scheme when it is truncated. This might be the case, given the phenomenological success of the scheme for inclusive photon, electron, pion, and (anti-)neutrino reactions at intermediate energies [18,25,28,29]. In addition, we have pointed out that 1p1h or 1p1h1π W-absorption modes in the primary vertex may also lead to two-nucleon final states, due to SNC. In fact, we have discussed some medium corrections to the 1p1h mechanism (see left diagram in Fig. 4), which can be interpreted as an interference between amplitudes involving one- and two-nucleon currents. Such mechanisms might be significant for inclusive cross sections [8,14] and also give rise to visible signatures of two-nucleon final states, due to subsequent collisions suffered by the primary nucleon as it travels out through the nucleus. These contributions have not been considered in the analysis carried out in this work. They would likely provide nucleon distributions that can be understood in terms of their QE origin and which might well be separated from those studied in this work, where the Δ resonance is excited or 3p3h components are sizable.

ACKNOWLEDGMENTS

This work was supported by the Swiss National Foundation Grant No. 200021_85012; the Spanish Ministerio de Economia y Competitividad and the European Regional Development Fund under Contract No. FIS2017-84038-C2-1-P; the EU STRONG-2020 project under the program H2020-INFRAIA-2018-1, Grant No. 824093; the Cluster of Excellence "Precision Physics, Fundamental Interactions, and Structure of Matter (PRISMA$^+$)," funded by the German Research Foundation (DFG) within the German Excellence Strategy (Project ID 39083149); and by the DFG-funded Collaborative Research Center SFB 1044.

[1] L. Alvarez-Ruso *et al.*, Prog. Part. Nucl. Phys. **100**, 1 (2018).
[2] J. Nieves, F. Sanchez, I. R. Simo, and M. J. Vicente Vacas, Phys. Rev. D **85**, 113008 (2012).
[3] L. Alvarez-Ruso, Y. Hayato, and J. Nieves, New J. Phys. **16**, 075015 (2014).
[4] A. Lovato, S. Gandolfi, R. Butler, J. Carlson, E. Lusk, S. C. Pieper, and R. Schiavilla, Phys. Rev. Lett. **111**, 092501 (2013).
[5] A. A. Aguilar-Arevalo *et al.* (MiniBooNE), Phys. Rev. D **81**, 092005 (2010).
[6] A. Aguilar-Arevalo *et al.* (MiniBooNE), Phys. Rev. D **88**, 032001 (2013).
[7] K. Abe *et al.* (T2K), Phys. Rev. D **93**, 112012 (2016).
[8] A. Lovato, J. Carlson, S. Gandolfi, N. Rocco, and R. Schiavilla (unpublished).
[9] M. Martini, M. Ericson, G. Chanfray, and J. Marteau, Phys. Rev. C **80**, 065501 (2009).
[10] M. Martini, M. Ericson, G. Chanfray, and J. Marteau, Phys. Rev. C **81**, 045502 (2010).
[11] E. Oset and L. L. Salcedo, Nucl. Phys. A **468**, 631 (1987).
[12] K. Shimizu and A. Faessler, Nucl. Phys. A **333**, 495 (1980).
[13] W. M. Alberico, M. Ericson, and A. Molinari, Ann. Phys. **154**, 356 (1984).
[14] O. Benhar, A. Lovato, and N. Rocco, Phys. Rev. C **92**, 024602 (2015).
[15] N. Rocco, C. Barbieri, O. Benhar, A. De Pace, and A. Lovato, Phys. Rev. C **99**, 025502 (2019).
[16] E. Hernandez, J. Nieves, and M. Valverde, Phys. Rev. D **76**, 033005 (2007).
[17] G. D. Megias, J. E. Amaro, M. B. Barbaro, J. A. Caballero, T. W. Donnelly, and I. R. Simo, Phys. Rev. D **94**, 093004 (2016).
[18] J. Nieves, I. R. Simo, and M. J. Vicente Vacas, Phys. Rev. C **83**, 045501 (2011).
[19] J. Nieves, I. Ruiz Simo, and M. J. Vicente Vacas, Phys. Lett. B **707**, 72 (2012).
[20] J. Nieves, I. Ruiz Simo, and M. J. Vicente Vacas, Phys. Lett. B **721**, 90 (2013).
[21] Y. Hayato, Acta Phys. Pol. B **40**, 2477 (2009).
[22] E. Hernandez and J. Nieves, Phys. Rev. D **95**, 053007 (2017).
[23] S. Dolan, G. D. Megias, and S. Bolognesi, Phys. Rev. D **101**, 033003 (2020).
[24] J. Carlson, J. Jourdan, R. Schiavilla, and I. Sick, Phys. Rev. C **65**, 024002 (2002).
[25] E. Oset, H. Toki, and W. Weise, Phys. Rep. **83**, 281 (1982).
[26] J. Speth, E. Werner, and W. Wild, Phys. Rep. C **33**, 127 (1977).
[27] J. Speth, V. Klemt, J. Wambach, and G. Brown, Nucl. Phys. A **343**, 382 (1980).
[28] A. Gil, J. Nieves, and E. Oset, Nucl. Phys. A **627**, 543 (1997).
[29] R. C. Carrasco and E. Oset, Nucl. Phys. A **536**, 445 (1992).

[30] J. Nieves, E. Oset, and C. Garcia-Recio, Nucl. Phys. A **554**, 554 (1993).
[31] H. Kamano, S. X. Nakamura, T. S. H. Lee, and T. Sato, Phys. Rev. C **88**, 035209 (2013).
[32] A. Matsuyama, T. Sato, and T. S. H. Lee, Phys. Rep. **439**, 193 (2007).
[33] T. Sato and T.-S. H. Lee, Phys. Rev. C **54**, 2660 (1996).
[34] T. Sato and T. S. H. Lee, Phys. Rev. C **63**, 055201 (2001).
[35] T. Sato, D. Uno, and T. S. H. Lee, Phys. Rev. C **67**, 065201 (2003).
[36] T. Sato and T. S. H. Lee, J. Phys. G **36**, 073001 (2009).
[37] J. E. Sobczyk, E. Hernández, S. X. Nakamura, J. Nieves, and T. Sato, Phys. Rev. D **98**, 073001 (2018).
[38] J. Nieves, Czech. J. Phys. **46**, 673 (1996).
[39] T. E. O. Ericson and W. Weise, *Pions and Nuclei* (Clarendon Press, Oxford, UK, 1988), Vol. 74.
[40] J. Nieves, I. R. Simo, F. Sánchez, and M. J. V. Vacas, JPS Conf. Proc. **12**, 010002 (2016).
[41] O. Buss, T. Gaitanos, K. Gallmeister, H. van Hees, M. Kaskulov, O. Lalakulich, A. Larionov, T. Leitner, J. Weil, and U. Mosel, Phys. Rep. **512**, 1 (2012).
[42] O. Benhar, N. Farina, H. Nakamura, M. Sakuda, and R. Seki, Phys. Rev. D **72**, 053005 (2005).
[43] O. Benhar, Phys. Rev. C **87**, 024606 (2013).
[44] E. Vagnoni, O. Benhar, and D. Meloni, Phys. Rev. Lett. **118**, 142502 (2017).
[45] J. Nieves and J. E. Sobczyk, Ann. Phys. **383**, 455 (2017).
[46] P. Fernandez de Cordoba and E. Oset, Phys. Rev. C **46**, 1697 (1992).
[47] E. Oset and W. Weise, Nucl. Phys. A **319**, 477 (1979).
[48] J. Nieves, J. E. Amaro, and M. Valverde, Phys. Rev. C **70**, 055503 (2004).
[49] V. Pascalutsa, Phys. Lett. B **503**, 85 (2001).
[50] L. Alvarez-Ruso, E. Hernández, J. Nieves, and M. J. Vicente Vacas, Phys. Rev. D **93**, 014016 (2016).
[51] L. L. Salcedo, E. Oset, M. J. Vicente-Vacas, and C. Garcia-Recio, Nucl. Phys. A **484**, 557 (1988).
[52] E. S. Pinzon Guerra *et al.*, Phys. Rev. D **99**, 052007 (2019).
[53] R. Gran, J. Nieves, F. Sanchez, and M. J. Vicente Vacas, Phys. Rev. D **88**, 113007 (2013).
[54] P. A. Rodrigues *et al.* (MINERvA), Phys. Rev. Lett. **116**, 071802 (2016); **121**, 209902 (2018).